

CHARACTERISTICS OF SMALL-SCALE MAGNETIC FLUCTUATIONS OVER THE HIGH-LATITUDE IONOSPHERE

Toshihiko IYEMORI, Tatsuya IKEDA and Akinari NAKAGAWA

*Data Analysis Center for Geomagnetism and Spacemagnetism, Faculty of Science,
Kyoto University, Kitashirakawa Oiwake-cho, Sakyo-ku, Kyoto 606*

Abstract: The global amplitude distributions of the small-scale ($1 < L < 35$ km) or short-time scale ($0.12 < T < 5$ s) magnetic fluctuations over the high-latitude ionosphere are obtained for various geomagnetic, seasonal and IMF conditions using the MAGSAT data and are compared with the large-scale Birkeland currents. On the dayside, the maximum of the amplitude distribution appears near the poleward edge of the large-scale Birkeland current region-1 or at the latitude poleward of it. The amplitude strongly depends on the ionospheric conductivity and varies about factor three or more even in the same conditions of the geomagnetic activity, suggesting that the fluctuations are generated mainly by small-scale Birkeland currents rather than by Alfvén waves. The IMF- B_y causes the dawn-dusk asymmetry of the amplitude and the IMF- B_z controls the latitudinal distribution of the fluctuations. On the night-side, the amplitude is controlled mainly by the geomagnetic activity, and the active region statistically corresponds to the large scale Birkeland current regions. However, the correlation between the amplitude and the large-scale Birkeland current density is not necessarily good. On both sides, the latitude of the maximum amplitude roughly correspond to that of the large-scale magnetospheric convection reversal, suggesting that the small-scale Birkeland currents originate from the turbulence generated in the strong convection shear regions.

1. Introduction

The small-scale ($L < 80$ km) or short-time scale ($T < 10$ s) magnetic fluctuations superposed on or independent of the large-scale Birkeland currents have been observed by the MAGSAT or by other low-altitude satellites such as the Dynamics Explorer-2 (SUGIURA *et al.*, 1982, 1984) or TRIAD (SAFLEKOS *et al.*, 1978). The significance of them has been also pointed out from viewpoints of solar wind-magnetosphere interaction, magnetosphere-ionosphere coupling, energy deposition to the ionosphere or plasma instabilities (SAFLEKOS *et al.*, 1978; SUGIURA *et al.*, 1982, 1984; GURNETT *et al.*, 1984). As for the electromagnetic energy deposition to the ionosphere, the amount of energy associated with the small-scale fluctuations may be much smaller than that associated with the large-scale Birkeland currents. However, it can be comparable to the energy associated with the particle precipitation (*e.g.* GURNETT *et al.*, 1984).

SUGIURA *et al.* (1984) emphasized from the Dynamics Explorer-2 magnetic field measurement that the Birkeland currents are highly structured and that the current density is sometimes very high ($> 100 \mu\text{A}/\text{m}^2$). SUGIURA *et al.* (1982) and SUGIURA (1984) also found that the correlation between the electric field and the magnetic field

perpendicular to it is generally good even for small-scale fluctuations. They explained their results as an evidence of meridional current closure of quasi-static Birkeland currents through the ionospheric Pederson current.

On the other hand, GURNETT *et al.* (1984) reported that the short-period magnetic and electric field fluctuations observed by the Dynamics Explorer-1 showed a relation consistent with that of the propagating Alfvén waves. Therefore, the origin of the small scale fluctuations is probably not unique and the actual fluctuations observed along the satellite orbits may be a complex combination of the Birkeland currents and the Alfvén waves, and the ratio of the combination may be a function of the scale size, local time, geomagnetic activity, etc.

SAFLEKOS *et al.* (1978) examined the appearance probability of the transverse magnetic field fluctuations which are observed over the polar caps and which have a time scale around 10 s using the TRIAD magnetic field data. They found that the interplanetary magnetic field east-west component (IMF- B_y) causes a clear asymmetry of the appearance probability between northern and southern polar caps. However, the origin of them is not clear.

Generally speaking, the amplitude of the fluctuations is smaller for smaller scale size, and that of the time scale around 1 s is usually in the order of a few nT. As the magnetometer of the MAGSAT has a step size of 0.5 nT/step, it is possible to analyze the small-scale magnetic fluctuations with a scale size of a few seconds (*cf.* the step sizes of the DE-2 and the TRIAD are 3 and 12 nT/step, respectively). In this paper, we analyze the magnetic fluctuations of time scale less than 5 s using the MAGSAT data and examine the effects of the ionospheric conductivity, geomagnetic activity, large-scale Birkeland current density and the interplanetary magnetic fields to the amplitude of the fluctuations and their global distribution.

2. Method and Analysis

The vector magnetic field data obtained by the MAGSAT have a sampling rate of 16 samples/s and a resolution of 0.5 nT/step (LANGEL *et al.*, 1981). The standard deviation (σ) of successive 80 data points was used as a measure of fluctuations for 5-s interval. We also used the time change rate of 5-s average Y component, from which the earth's main model field is subtracted, as a measure of large scale Birkeland current density. The standard deviation recorded on the MAGSAT Investigator-B magnetic tapes was calculated for each vector component from residuals after slow variation over 5 s which were subtracted by a linear regression procedure (see LANGEL *et al.*, 1981). The vector components are expressed in the geographic coordinate system (*i.e.* X ;north, Y ;east, Z ;downward).

If we assume that the slow variations (*i.e.* time scale greater than 5 s) indicate the static structure of large-scale Birkeland currents along the MAGSAT orbit, the time change rate of the Y component should be roughly proportional to the density of large-scale Birkeland currents, because the large scale Birkeland currents tend to show a sheet structure and the direction of the sheet tends to be east-west rather than north-south. To calculate the time change rate ($\nabla \delta_y$), we used three successive data points of 5-s average data, and a parabola was fitted to them to calculate gradient at

the middle point. Therefore, the time change rate approximated as above should be proportional to the average current density of spatial scale about 35 km.

The standard deviation is a measure of the power of the magnetic fluctuations of time scale between 1/8 and 5 s or spatial scale approximately between 1 and 35 km along the orbit. The power spectral peaks in this range vary from one case to another, but generally speaking, the fluctuations of period greater than a few seconds mainly contribute to the standard deviation.

The data period which we used is from January 19, 1980 through May 19, 1980. The standard deviations were sorted by the IMF direction and geomagnetic activity and averaged over in each $1^\circ \times 1^\circ$ mesh to obtain a global amplitude distribution. The invariant latitude (INV) and 'invariant' magnetic local time (MLT) were used (see ARAKI *et al.*, 1984). The hourly average ISEE-3 IMF data were added to the data set in the interplanetary medium data book tape by KING (1983), and the resultant rate of the IMF data coverage for the MAGSAT period was 90%. Hourly average *AE* indices were also used.

3. Results

Figure 1 shows an example of the magnetic field variations observed by the MAGSAT along its orbit near the polar cusp region. The lower two traces are the hor-

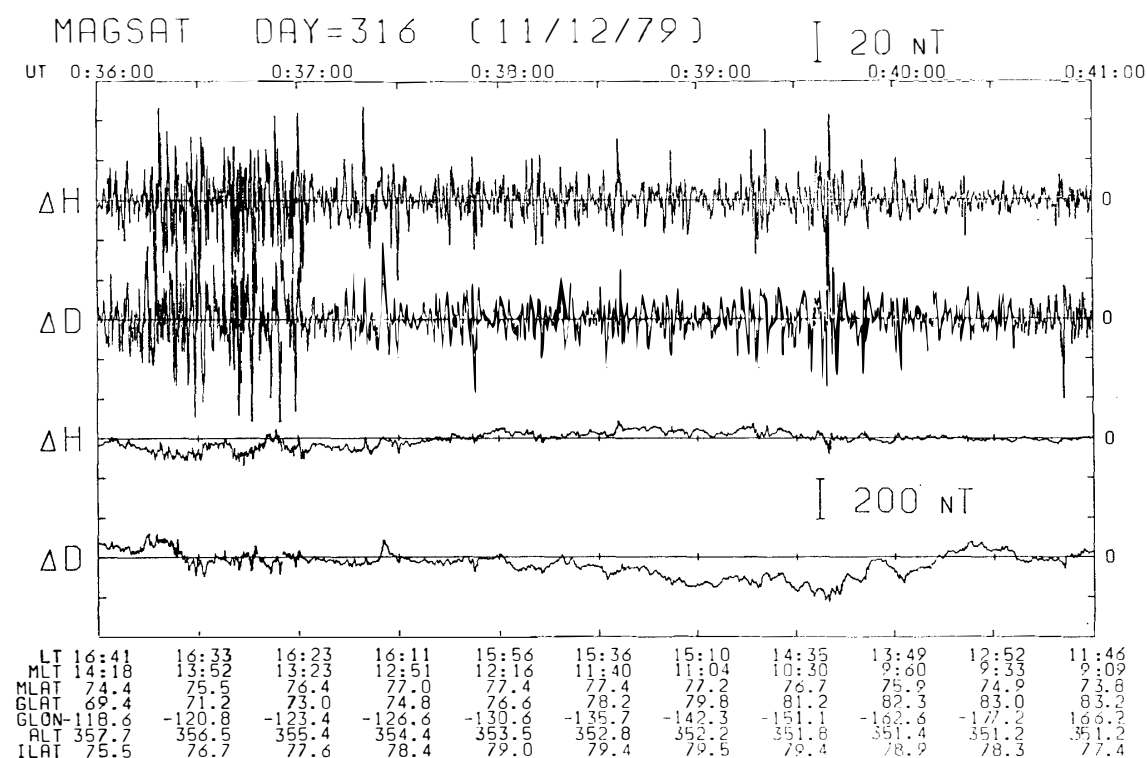


Fig. 1. An example of small-scale magnetic fluctuations observed by the MAGSAT along its orbit over the dayside cusp region. The upper two traces present the high-pass filtered data for the lower two traces. The cutoff frequency is about 5 s. Note for the difference of vertical scale between the upper two and the lower two traces.

horizontal (positive northward) and the east-west component of the disturbance field, respectively. The upper two traces are the high-pass filtered data for the lower two traces. As we see in Fig. 1, there exist the small-scale magnetic fluctuations throughout the cusp region and the amplitude of them is around 20 nT. The cutoff frequency of the filter used for this example is about 5 s. Therefore, to use the standard deviation of 5-s interval is approximately equivalent to take the power of the high-pass filtered fluctuations such as shown in Fig. 1.

Figure 2 (upper panel) shows the amplitude distribution of σ_y sorted by the AL index. The characteristics of the distribution for the X component, σ_x , are essentially the same with those for σ_y , except in the region near 06 and 18 MLT where σ_y is greater than σ_x . The lower panel shows the average position of large-scale region-1 and -2 Birkeland currents obtained by IJIMA and POTEMRA (1978) using the TRIAD data. Although it could be debatable, even for the same AL level, to compare the position statistically determined from two different data sets, we see some differences between the distribution of the small-scale fluctuations and the large-scale Birkeland currents. When the $|AL|$ is small (right), the σ_y is large around the cusp region poleward of the region-1 current and it is small on the night side. On the other hand, when the AL is large (left), the large σ_y region roughly correspond to the large-scale Birkeland cur-

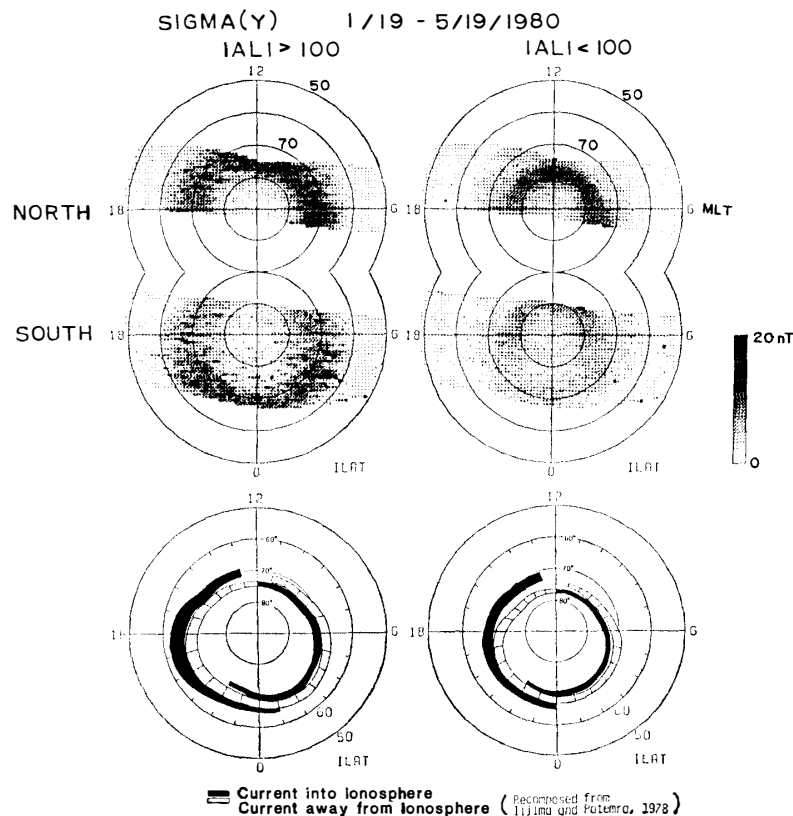


Fig. 2. Amplitude distribution of the standard deviation of the east-west component (upper panel) and the statistical distribution of the large-scale Birkeland currents obtained by IJIMA and POTEMRA (1978) (lower panel). Data were averaged over $1^\circ \times 1^\circ$ mesh. Results for quiet geomagnetic conditions ($|AL| < 100$ nT, right) and disturbed conditions ($|AL| > 100$ nT, left) are shown.

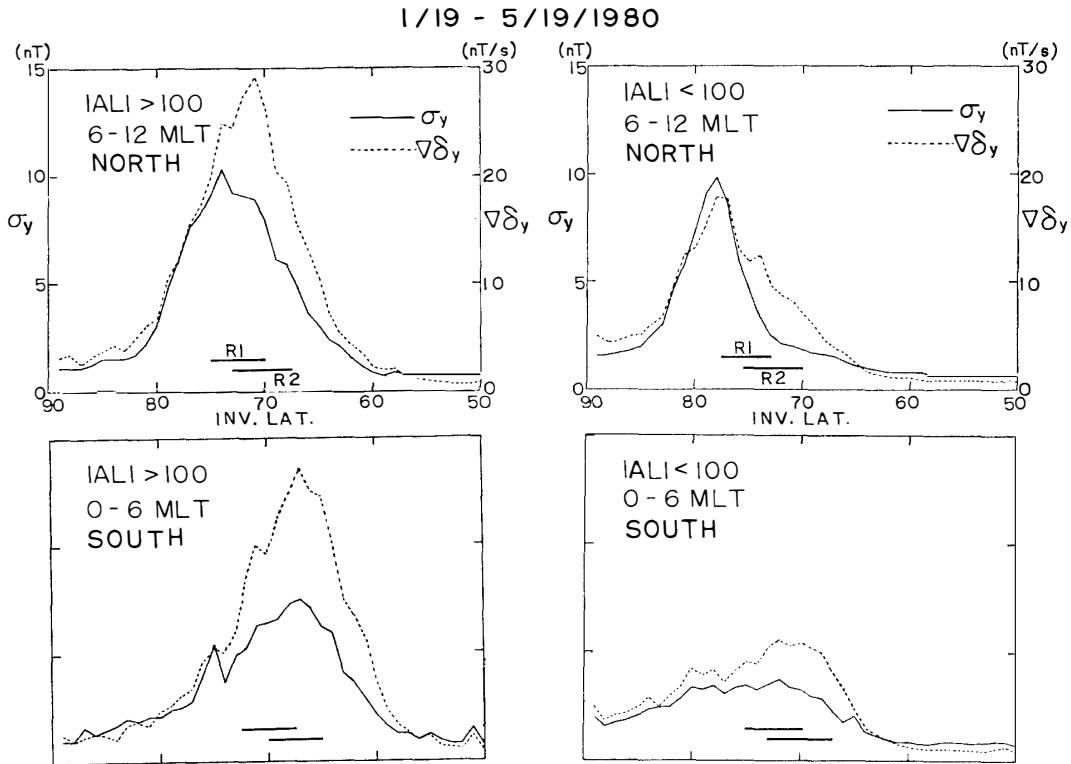


Fig. 3. Latitudinal distribution of the standard deviation, σ_y , and the time change rate of the 5-s average Y component which is roughly proportional to the large-scale Birkeland current density. These quantities were averaged in the local time sector indicated in each panel.

rent region, and the σ_y is not small even on the nightside. These characteristics are more clearly seen in Fig. 3.

In Fig. 3, the latitudinal distributions of the σ_y and the $\nabla\delta_y$ are shown. The right two panels are for quiet geomagnetic condition and the left panels are for disturbed condition. The solid-lines denote the longitudinally averaged σ_y within a local time sector indicated in each panel. The dotted lines denote the averaged $\nabla\delta_y$. The horizontal thick bars indicate the latitudinal range of region-1 (R1) and region-2 (R2)

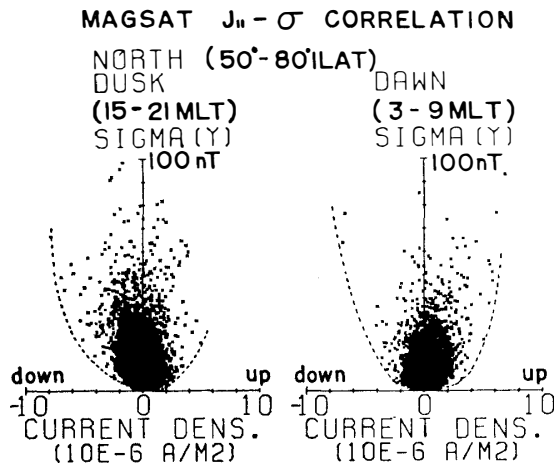


Fig. 4. Correlation plot between the standard deviation, σ_y , and the large-scale Birkeland current density which was calculated from the time change rate of the 5-s average Y-component. The results for the dawn and dusk local time sectors are shown.

Birkeland currents obtained by IJIMA and POTESRA (1978) as also shown in Fig. 2. On the dayside (6–12 MLT), the peaks of both the σ_y and $\nabla\delta_y$ correspond to the poleward edge of the region-1 current. However, the shape of meridional distribution is different between these two parameters. That is, the $\nabla\delta_y$, which is roughly proportional to the large-scale current density, does not decrease toward the low-latitude side so rapidly as the σ_y . For the disturbed condition, the peak of the $\nabla\delta_y$ is near the border between the region-1 and -2, though the peak of the σ_y is still near the poleward edge of the region-1. On the night-side, the σ_y is nearly proportional to the $\nabla\delta_y$ and the magnitude of them is strongly controlled by the geomagnetic activity as is also seen in Fig. 2. The peaks of them are near the border between the region-1 and -2.

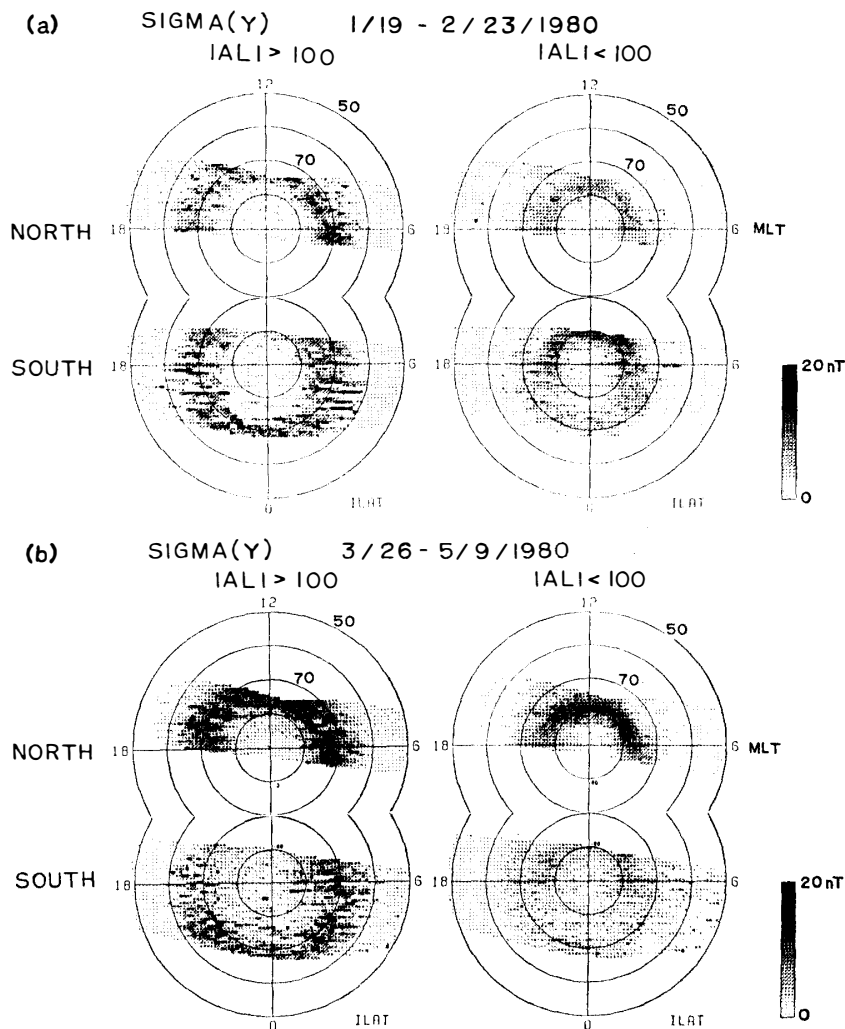


Fig. 5. Amplitude distribution of the standard deviation of the east-west component. Data were averaged over $1^\circ \times 1^\circ$ mesh. Results for quiet geomagnetic conditions ($|AL| < 100$ nT, right) and disturbed conditions ($|AL| > 100$ nT, left) are shown. (a) The satellite orbit is approximately along the day/night terminator or slightly tilted toward the sun in the southern hemisphere. (b) The orbit over the southern polar region is in the daylight hemisphere and the northern orbit is in the dark hemisphere. The amplitude greatly increases in the daylight hemisphere.

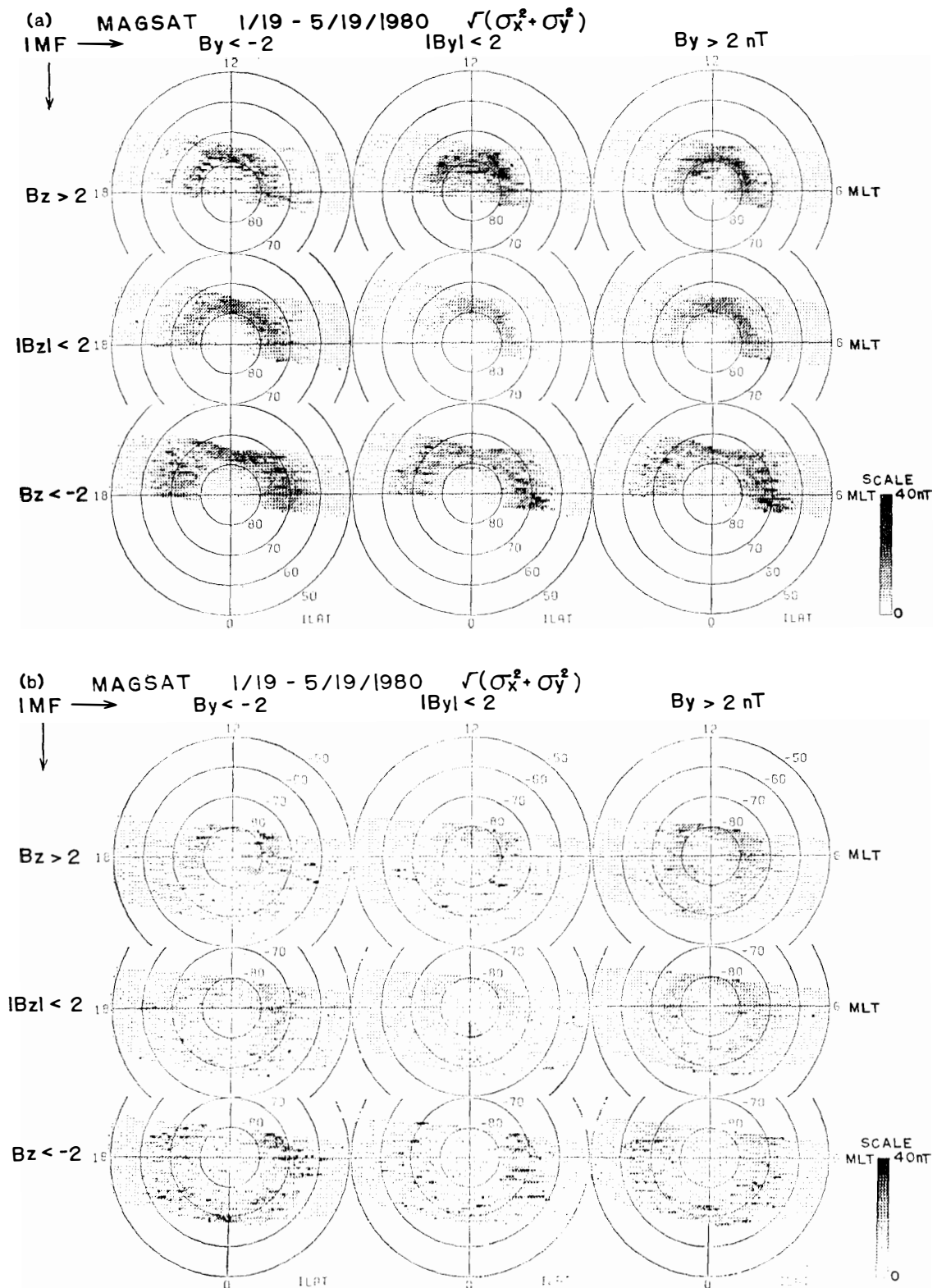


Fig. 6. Amplitude distribution of the standard deviation sorted by the IMF direction. The geometric mean of the standard deviation for the north-south and the east-west components is used. Results for the (a) northern and (b) southern hemisphere are shown. The IMF- B_y effect appears as a dawn-dusk asymmetry of the active region.

Figure 4 is a correlation plot between the σ_y (vertical axis) and the current density of large-scale Birkeland current (horizontal axis). We do not see any clear correlation between these two parameters. However, the σ_y is not small when the large-scale current density is high as shown by the broken line. There is a tendency that the large σ_y is more frequent in the upward current region on the dawn-side and in the downward current region on the dusk side.

Figure 5 shows the distribution of the σ_y over the northern and southern polar regions in different seasons. Figure 5a is for the period when the MAGSAT orbit lies nearly along the day/night terminator or slightly on the dayside of it in the southern hemisphere. Figure 5b is for the case when the northern passes are in the daylight hemisphere and the southern passes are in the dark hemisphere. The standard deviations on the dayside are clearly enhanced when the orbit is in the daylight hemisphere. On the other hand, the active region on the nightside roughly corresponds to the large-scale Birkeland current region-1 and -2, and the amplitude strongly depends on the geomagnetic activity rather than on the ionospheric conductivity.

Figure 6 shows the IMF- Y and $-Z$ dependence of the distribution of $\sqrt{(\sigma_x^2 + \sigma_y^2)}$. Results for the northern hemisphere are shown in Fig. 6a and those for the southern hemisphere in Fig. 6b. The number of passes in one $1^\circ \times 1^\circ$ mesh for each IMF direction is, roughly speaking, about 10 passes for the northern hemisphere and about 5 passes for the southern hemisphere. In the following, we discuss the IMF effect on the distribution in the northern hemisphere only because of the problem in the statistical reliability of that in the southern hemisphere. The IMF- B_z mainly controls the latitudinal distribution. As the B_z becomes negative (*i.e.* southward), the active region shifts equatorward and broadens. However, the maximum amplitude is of the same level as for northward IMF. The amplitude is small in the case of $|B_y| < 2\text{nT}$ and $|B_z| < 2\text{nT}$ (the central panel in Fig. 6a), suggesting a weak interaction between the solar wind and the magnetosphere in weak IMF conditions. The IMF- B_y controls the distribution in the dawn-dusk direction. One remarkable signature is the appearance of two active regions (speak) around 09 and 15 MLT at 78° INV when $|B_y| < 2\text{nT}$ and $B_z > 2\text{nT}$. When $B_y > 2\text{nT}$ and $B_z > 2\text{nT}$, the peak around 09 MLT still exists and the peak near 15 MLT disappears. When $B_y < -2\text{nT}$ and $B_z > 2\text{nT}$, the peak around 09 MLT disappears and the peak on the afternoon side seems to remain.

For $B_z > 2\text{nT}$ (*i.e.* northward IMF) cases, another active region appears around 82° INV (*i.e.* over the polar cap). However, the IMF- B_y effect is in the opposite sense to that for the distribution around 78° INV. That is, a clear peak appears on the afternoon side (~ 15 MLT) when $B_y > 2\text{nT}$. When $|B_y| < 2\text{nT}$, it appears around noon (10–14 MLT). The peak is not clear when $B_y < -2\text{nT}$ because of the data gap around 80° INV and ~ 10 MLT, but seems to exist between 10 and 12 MLT.

4. Discussion

It is difficult to identify the origin of the small-scale magnetic fluctuations from magnetic field data only. However, a clear seasonal variation of the amplitude (see Fig. 5) suggests that these fluctuations which contribute to the standard deviations

for 5-s intervals are caused by small-scale Birkeland current structures rather than by Alfvén waves for the following reason: For the case of static Birkeland currents, the amplitude of the fluctuations should be proportional to the ionospheric Pederson conductivity if the amplitude of the electric field fluctuations remain at the same level for the same AL conditions. On the other hand, the effect of the reflection coefficient at the ionosphere on wave amplitude should be within a factor $\sqrt{2}$ if we assume a single reflection and the same amplitude for the incident waves for the same AL conditions. The mean amplitude near the dayside maximum (*e.g.* $\sim 78^\circ$ INV and ~ 8 MLT) differs by about factor of three or more between the northern and southern hemispheres for the case of Fig. 6b, supporting the explanation as the small-scale Birkeland currents. The clear seasonal variation also suggests that the generation of the small-scale current system is, more or less, constant voltage type rather than constant current type (*cf.* LYSAK, 1985).

The tendency that the σ_y is generally greater than the σ_x in the dawn (1–9 MLT) or in the dusk (15–23 MLT) sector but they are almost comparable in the noon sector (9–15 MLT) or near the midnight (23–01 MLT) suggests that the small-scale Birkeland current structure tends to be the sheet type which extends in the east-west direction in the dawn and dusk sectors. This tendency is more clear in the dusk sector than that in the dawn sector, indicating the difference in the structure of the fluctuations.

The facts that the σ_y is generally large (~ 20 nT) in the polar cusp region even in the quiet geomagnetic condition and that the peak of the latitudinal distribution is near the poleward edge of the Birkeland current region-1 suggest that the small-scale magnetic fluctuations near the cusp region are more directly related to the solar wind-magnetosphere interaction rather than to the internal disturbance like the magnetospheric substorms. On the nightside, however, the σ_y is strongly controlled by the geomagnetic activity and the region of large σ_y roughly corresponds to the large-scale Birkeland current region, indicating that the small-scale fluctuations are generated in the large-scale Birkeland current region by the internal disturbance of the magnetosphere and/or that the ionospheric conductivity enhanced by the precipitating electrons controls the amplitude of the fluctuations.

On the other hand, the large σ regions also approximately correspond to the large-scale magnetospheric convection reversals where the convection shear motion is supposed to be strong. (*e.g.* compare Figs. 2 and 6 with Fig. 8 in HEELIS *et al.*, 1980 and Fig. 4 in FRIIS-CHRISTENSEN *et al.*, 1985, respectively, or compare the case of $|B_y| < 2$ nT and $B_z > 2$ nT in our Fig. 6a with Fig. 4a in ARAKI *et al.*, 1984). The large-scale Birkeland current density is usually high at the reversal. The difference of the latitudinal distribution between the σ_y and the large-scale current density on the dayside (see Fig. 3) might be explained as follows: The large-scale Birkeland current density is controlled by the gradient of the convection electric field (*i.e.* convection shear) and the ionospheric conductivity (FUJII *et al.*, 1981; SUGIURA *et al.*, 1982, 1984), but the small-scale Birkeland currents are generated in the limited region of strong convection shear. On the dayside, the ionospheric conductivity is mainly determined by the solar EUV radiation, and it is higher in the lower latitude. Therefore, the large-scale current density does not decrease so rapidly as the small-scale fluctuations toward the lower latitude even if the gradient of convection electric field decreases.

The distribution and its IMF- B_y dependence of the soft electron precipitation for $B_z > 0$ obtained by CANDIDI *et al.* (1983) are similar to those of the small-scale magnetic fluctuations (*i.e.* Fig. 6a), suggesting a close connection of the soft electron precipitation with the small scale Birkeland currents.

The statistical proportionality between the σ_y and the $\nabla \delta_y$ in Fig. 3 on the night-side indicates that the small-scale fluctuations are generated in the region where the large-scale Birkeland currents are also generated. The correlation plot between the σ_y and the $\nabla \delta_y$ (Fig. 4) indicates that the small-scale fluctuations are not necessarily related to the high density region of large-scale Birkeland current, but the high density region of large-scale Birkeland currents always accompanies the large amplitude fluctuations. The statistical coincidence of large-scale and small-scale Birkeland current regions might be a consequence of the coincidence of high conductivity region generated by particle precipitation and strong convection shear region.

The generation mechanism of the Birkeland currents in the magnetosphere is related to the plasma motion (vorticity or acceleration) or the spatial gradient of the plasma parameters (see HASEGAWA and SATO, 1980). Therefore, if the small-scale fluctuations mainly come from quasi-static Birkeland currents which are generated in the equatorial region of the magnetosphere, the scale size and the amplitude of the fluctuations give us the information on the turbulence in the magnetospheric plasma. And our results of analysis suggest that the turbulence is generated in the strong convection shear region and the convection shear on the dayside is controlled by the IMF direction and that on the nightside is controlled by the geomagnetic activity.

Acknowledgments

This work has been carried out by the use of MAGSAT data provided by NASA to the Japanese MAGSAT investigation team for the approved Statement of Work M43. The IMF data were provided by J. H. KING and by E. J. SMITH through the WDC-A for Rocket and Satellites, GSFC, NASA. The AE indices were obtained from the WDC-C2 for Geomagnetism, Kyoto University. We wish to thank Dr. M. SUGIURA at NASA/GSFC and Dr. T. ARAKI, Mr. T. KAMEI and Mr. M. YAMAUCHI at our institute for their useful discussions.

References

- ARAKI, T., KAMEI, T. and IYEMORI, T. (1984): Polar cap vertical currents associated with northward interplanetary magnetic field. *Geophys. Res. Lett.*, **11**, 23–26.
- CANDIDI, M., KROEHL, H. W. and MENG, C.-I. (1983): Intensity distribution of dayside polar soft electron precipitation and the IMF. *Planet. Space. Sci.*, **31**, 489–498.
- FRIIS-CHRISTENSEN, E., KAMIDE, Y., RICHMOND, A. D. and MATSUSHITA, S. (1985): Interplanetary magnetic field control of high-latitude electric fields and currents determined from Greenland magnetometer data. *J. Geophys. Res.*, **90**, 1325–1338.
- FUJII, R., IJIMA, T., POTEIRA, T. A. and SUGIURA, M. (1981): Seasonal dependence of large-scale Birkeland currents. *Geophys. Res. Lett.*, **10**, 1103–1106.
- GURNETT, D. A., HUFF, R. L., MENIETTI, J. D., BURCH, J. L., WINNINGHAM, J. D. and SHAWHAN, S. D. (1984): Correlated low-frequency electric and magnetic noise along the auroral field lines. *J. Geophys. Res.*, **89**, 8971–8985.

- HASEGAWA, A. and SATO, T. (1980): Generation of field-aligned current during substorms. *Dynamics of the Magnetosphere*, ed. by S.-I. AKASOFU. Dordrecht, D. Reidel, 529–542.
- HEELIS, R. A., WINNINGHAM, J. D., HANSON, W. B. and BURCH, J. L. (1980): The relationships between high-latitude convection reversals and the energetic particle morphology observed by Atmospheric Explorer. *J. Geophys. Res.*, **85**, 3315–3324.
- IJIMA, T. and POTEIRA, T. A. (1978): Large-scale characteristics of field-aligned currents associated with substorms. *J. Geophys. Res.*, **83**, 599–615.
- KING, J. H. (1983): *Interplanetary Medium Data Book—Supplement 2 1978–1982*, NSSDC/WDC-A-R&S 83-01, NASA/GSFC, Greenbelt, Maryland.
- LANGEL, R., BERBERT, J., JENNINGS, T. and HORNER, R. (1981): *MAGSAT Data Processing: A Report for Investigators*. Tech. Mem. 82160, NASA/GSFC, Greenbelt, Maryland.
- LYSAK, R. L. (1985): Auroral electrodynamics with current and voltage generators. *J. Geophys. Res.*, **90**, 4178–4190.
- SAFLEKOS, N. A., POTEIRA, T. A. and IJIMA, T. (1978): Small-scale transverse magnetic disturbances in the polar regions observed by Triad. *J. Geophys. Res.*, **83**, 1493–1502.
- SUGIURA, M. (1984): A fundamental magnetosphere—ionosphere coupling mode involving field-aligned currents as deduced from DE-2 observations. *Geophys. Res. Lett.*, **11**, 877–880.
- SUGIURA, M., IYEMORI, T., HOFFMAN, R. A., MAYNARD, N. C., BURCH, J. L. and WINNINGHAM, J. D. (1984): Relationships between field-aligned currents, electric fields, and particle precipitation as observed by Dynamics Explorer-2. *Magnetospheric Currents*, ed. by T. A. POTEIRA. Washington, D.C., Am. Geophys. Union, 96–103 (*Geophys. Monograph 28*).
- SUGIURA, M., MAYNARD, N. C., FARTHING, W. H., HEPPNER, J. P. and LEDLEY, B. G. (1982): Initial results on the correlation between the magnetic and electric fields observed from the DE-2 satellite in the field-aligned current regions. *Geophys. Res. Lett.*, **9**, 985–988.

(Received July 31, 1985; Revised manuscript received February 14, 1986)